Parameter transferability, self-doping, and metallicity in $LaNiO_3/LaMnO_3$ superlattices

Alejandro Lopez-Bezanilla,[1,2,*] Louis-François Arsenault,[3] Anand Bhattacharya,[2]
Peter B. Littlewood,[2,4] and Andrew J. Millis[3]
[1]*Theoretical Division, Los Alamos National Laboratory, Los Alamos, New Mexico 87545, USA*
[2]*Materials Science Division, Argonne National Laboratory, Lemont, Illinois 60439, USA*
[3]*Department of Physics, Columbia University, New York, New York 10027, USA*
[4]*James Franck Institute, University of Chicago, Chicago, Illinois 60637, USA*

(Received 4 April 2017; revised manuscript received 4 September 2018; published 17 January 2019)

Motivated by recent experiments, we use the $+U$ extension of the generalized gradient approximation to density functional theory to study superlattices composed of alternating layers of $LaNiO_3$ and $LaMnO_3$. For comparison we also study a rocksalt [(111) double perovskite] structure and bulk $LaNiO_3$ and $LaMnO_3$. A Wannier function analysis indicates that band parameters are transferable from bulk to superlattice situations with the exception of the transition-metal d-level energy, which has a contribution from the change in d-shell occupancy. The charge transfer from Mn to Ni is found to be moderate in the superlattice, indicating metallic behavior, in contrast to the insulating behavior found in recent experiments, while the rocksalt structure is found to be insulating with a large Mn-Ni charge transfer. We suggest a high density of cation antisite defects may account for the insulating behavior experimentally observed in short-period superlattices.

DOI: 10.1103/PhysRevB.99.035133

I. INTRODUCTION

The sensitive dependence of correlated electron properties on electron concentration and crystal structure has motivated the exploration of new systems that provide access to different regimes of the structure/concentration phase space. Oxide superlattices involving components with correlated electron properties are of particular interest because they present the possibility of controlled synthesis of correlated materials with specifically designed properties [1]. Efficient exploitation of the new materials fabrication capabilities to establish a broadly effective "materials by design" capability will be enhanced by the development and validation of theoretical methods and physical/chemical understanding of the relation between structure and correlated electron properties. Improved understanding of "transferability," the extent to which parameters established by study of a simpler system may be carried over to the description of a second, more complicated situation, is important to this process because, to the extent that parameters are transferrable, intuition obtained from studies of model system and simple bulk compounds can be used to guide synthesis and *ab initio* studies of complex structures.

In this paper we address the validation and transferability issues in the context of combinations of perovskite manganite ($LaMnO_3$, or LMO) and nickelate ($LaNiO_3$, or LNO) materials into superlattices. Individually, these transition-metal-oxide-based materials exhibit remarkable physical properties related to the interplay of magnetic, charge, orbital, and structural degrees of freedom, including colossal magnetoresistance, metal-insulator transitions, and orbital and spin-ordered states [2]. Chemical doping, pressure, and magnetic and electric fields have been employed to tune manganites and nickelates from one phase to another [3–5]. Gibert *et al.* [6], Piamonteze and coworkers [7], and Hoffman *et al.* [8] have studied interfaces between LNO and LMO experimentally. Gibert and coworkers [6] presented some density functional plus U studies of magnetic moments in (111) superlattices, and Lee and Han [9] studied charge transfer and magnetism. In related work, Zhong *et al.* [10] performed a maximally localized Wannier function (MLWF) analysis of $SrVO_3/SrTiO_3$ superlattices with the aim of constructing a model Hamiltonian to interpret the results of Yoshimatsu *et al.* [11,12]. These authors did not address the issues of parameter transferability. Our study builds on these works, presenting results related to parameter transferability and the physics of electron transfer in superlattices.

The present work is specifically motivated by the results of Hoffman *et al.* [13], who fabricated superlattices of the chemical formula $(LaNiO_3)_n(LaMnO_3)_n$ and showed transport and optical evidence of a metal-insulator transition occurring as n was decreased from 3 to 2. These authors further used x-ray spectroscopy to show a thickness-dependent transfer of electrons from Mn to Ni. Specifically, for a $(LNO)_2/(LMO)_2$ superlattice the cations exhibit spectra consistent with Mn^{4+} and Ni^{2+} oxidation states, very different from the nominal Mn^{3+} and Ni^{3+} oxidation states observed in the corresponding bulk materials, and they associated the electron transfer with the insulating behavior.

In this paper we report results of density functional theory and density functional theory plus U (DFT+U) calculations performed to help us understand the behavior of these materials and transition-metal oxides more generally. While DFT+U is a mean-field method that does not capture the full complexity of correlated electron materials, it does provide reasonable estimates of basic physics such as charge transfer,

*alejandrolb@gmail.com

allows for structural relaxation, and permits a detailed analysis of parameter transferability. We consider superlattices similar to those studied experimentally and for comparison also present results for the cubic ABO_3 perovskite and the rocksalt $A_2BB'O_6$ [(111) double perovskite]. We deal with idealized situations to get a sense of parameters and transferability and comment on the consequences of including more realistic details of the crystal structure. MLWFs [14] are employed to fit the band structures of the bulk compounds to tight-binding models which parametrize the Hamiltonian description of each compound. A comparison of parameters obtained from the Wannier fits indicates that the on-site energy and intersite hopping parameters are transferable (meaning that they take the same value as in the bulk parent compounds), with one exception: the transition-metal electronegativity is not transferable and instead depends on the degree of charge transfer. A related point was very recently made by Zhong and Hansmann [15], who introduced a model involving a combination of alignment of oxygen states and charge transfer. We discuss the relation of this work to ours in more detail below. These results indicate that insights from bulk materials can, to a very large degree, be carried over to the superlattice situation (making appropriate allowance for superlattice-induced changes in structure) but underscore the importance of an improved understanding of charge transfer and of the on-site energetics of the transition-metal ions.

Our results have implications for the interpretation of the experiments of Hoffman *et al.* [13]. In the layered situation the calculated charge transfer is much less than the one electron per Mn found experimentally, even after accounting for possible lattice relaxation; however, the charge transfer found for the rocksalt structure is closer to the experimental value, suggesting that the structures fabricated by Hoffman *et al.* have a high concentration of transition-metal antisite defects, as predicted by previous work [16], so that the actual experimental situation may correspond more closely to the rocksalt structure.

The rest of this paper is organized as follows. Section II presents the systems to be investigated and outlines the basic physics; Sec. III presents the model and calculational methods. Section IV discusses the energy bands that are the basic result. Section V presents an interpretation of the results. Section VI is a comparison to experiment. Section VII is a summary and conclusion.

II. MODEL

The systems studied are shown in Fig. 1. We consider the ideal cubic perovskite version of the bulk "parent compounds" $LaNiO_3$ and $LaMnO_3$ [Fig. 1(a)], a slightly idealized version of the superlattices (SL) studied experimentally [Fig. 1(b)], and a rocksalt [111 double perovskite structure (RS)] with interpenetrating Mn and Ni sublattices [Fig. 1(c)]. For most of our calculations we idealize the structures to minimize the number of parameters describing the electronic physics, thus enabling a straightforward interpretation of the computations.

We begin by describing the bulk parent compounds $LaNiO_3$ and $LaMnO_3$. $LaNiO_3$ [Fig. 1(a)] is the only one of the rare-earth nickelate perovskites that remains metallic and nonmagnetic down to the lowest temperatures (substituting another rare earth for La produces materials that have a low-temperature insulating phase characterized by a two-sublattice breathing distortion and by antiferromagnetism). $LaNiO_3$ forms in a slightly distorted version of the ideal ABO_3 perovskite structure, characterized by $R\bar{3}c$ symmetry and a pseudocubic lattice parameter of 3.83 Å. Here we approximate the structure as the simple cubic ABO_3 perovskite. Because we wish to compare to films grown on $SrTiO_3$ substrates, we will choose the lattice constant to be equal to the $SrTiO_3$ pseudocubic lattice constant of 3.95 Å. The relevant electronic states in $LaNiO_3$ are antibonding combinations of Ni d and O $2p\sigma$ orbitals. From the formal valence point of view, the Ni configuration is d^7 ($t_{2g}^6 - e_g^1$), making the material a representative spin-1/2, orbitally degenerate material. However, the highest-lying oxygen states are, in fact, believed to lie slightly higher in energy than the Ni e_g levels, placing the material in the "negative-charge-transfer" class of materials [17–20], so that the actual electronic configuration is closer to $d^8\bar{L}$, with Ni in the high-spin ($t_{2g}^6 - e_g^2$) state and one hole on the oxygen (ligand) network.

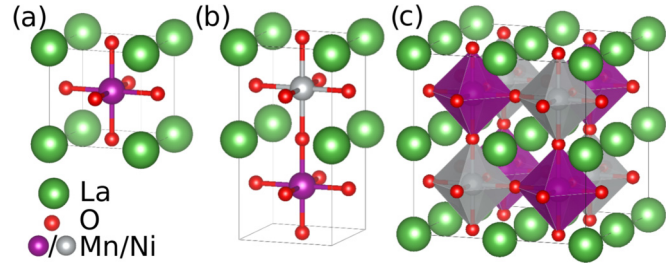

FIG. 1. Model representation of the structures studied in this paper. (a) Cubic $LaNiO_3$ or $LaMnO_3$, (b) multilayer of $[LaMnO_3]_1/[LaNiO_3]_1$, and (c) rocksalt structure of $LaMnO_3$ and $LaNiO_3$. In (c) the octahedra represent the sixfold coordination of the metallic cations.

Bulk $LaMnO_3$ is an antiferromagnetic insulator. Formal valence and Hund's coupling arguments indicate the Mn configuration is high-spin d^4 with half-filled fully spin polarized t_{2g}-symmetry orbitals contributing an electrically inert $S = 1$ "core spin" and the quarter-filled e_g manifold adding a potentially mobile $s = 1/2$ carrier whose spin is strongly aligned to the core spin [2,21,22]. In bulk $LaMnO_3$ [23,24], Jahn-Teller distortions involving alternating Mn-O bond lengths and $GdFeO_3$-type checkerboard tilting of the oxygen octahedra lift the orbital degeneracy of the e_g manifold, leading to an insulating ground state. Hole doping of $LaMnO_3$ reduces the tendency to Jahn-Teller order, and the fully hole doped end member $SrMnO_3$ is a cubic perovskite. Because we are interested in situations in which charge transfer occurs and because the Jahn-Teller ordering is, in many cases, suppressed in manganite films [25], we study the cubic-symmetry crystal structure [Fig. 1(a)]; again, for comparison to films we use the bulk $SrTiO_3$ lattice constant of 3.95 Å.

III. METHOD

A layered $(LaNiO_3)_n/(LaMnO_3)_n$ heterostructure (SL) may be formed by the periodic stacking of n two-dimensional layers of both $LaNiO_3$ and $LaMnO_3$ in the ideal perovskite

(001) direction. Figure 1(b) shows the $n = 1$ case, which we focus on in this paper for simplicity of interpretation. We note that this structure should show maximal charge transfer effects. To account for the strain induced by the substrate on which the experimental heterostructures were grown, the in-plane lattice parameters are fixed to the calculated bulk $SrTiO_3$ lattice constant of 3.95, and the out-of-plane lattice parameter is fixed to 2×3.95 Å. Rotation of the transition-metal-oxygen octahedra was not allowed. We considered three cases for internal coordinates: the apical O atoms at the same distance between the Mn and Ni atoms and displaced 0.2 and 0.4 Å towards Mn.

Finally, we studied an $A_2BB'O_6$ double-perovskite (rocksalt (RS)) structure [Fig. 1(c)] in which the six nearest cations to each Mn are Ni and vice versa. The Mn-Ni distance was again taken to be equal to the $SrTiO_3$ pseudocubic lattice constant of 3.95 Å. This structure is chosen to provide extra insight into the dependence of charge transfer on structure and also serves as a computationally tractable proxy for a superlattice with a very high density of cation antisite defects.

We use the DFT+U method, in which density functional band calculations are supplemented with on-site interactions among the transition-metal d orbitals. While DFT+U is a mean-field method that does not fully capture the complexities of correlated electron physics, it does adequately represent the basic energetics of materials, in particular capturing correctly the basic energetics associated with charge transfer. An important issue in this method is the choice of interaction parameters U and J and the corresponding double-counting correction. According to previously reported results [26], on-site intra-d interaction terms $U_{\mathrm{Mn}} = 4$ eV and $J_{\mathrm{Mn}} = 1.0$ eV provide an adequate description of $LaMnO_3$, successfully separating the higher-lying local minority-spin t_{2g} states from the local majority e_g bands above a band gap which is likewise increased. When used with the experimental low-temperature $Pbnm$ structure, this U_{Mn} produces results consistent with experiment. The on-site interaction terms for Ni have been chosen to be $U_{\mathrm{Ni}} = 6.0$ eV and $J_{\mathrm{Ni}} = 1.0$ eV, comparable to values used in the literature [27].

The fully localized limit double-counting correction was employed. This double- counting correction in effect compensates the Hartree shift of the transition-metal d orbital, fixing the relative electronegativities of the transition-metal and oxygen orbitals at about the values found in the density functional calculations.

The spin-polarized DFT calculations were performed using the projector augmented-wave method [28] and the Perdew-Burke-Ernzerhof generalized gradient approximation (GGA) exchange-correlation functional [29] with $+U$ corrections in the Dudarev *et al.* scheme [30] as implemented in the VASP code [31–33]. The rotationally invariant method with an effective $U_{\mathrm{eff}} = U - J$ was employed. The electronic wave functions were described using a plane-wave basis set with an energy cutoff of 500 eV. Atomic positions were fixed in the cubic or supercell geometries described in the previous section, with a lattice parameter of 3.95 Å. A $10 \times 10 \times 10\,k$-point sampling in Γ-centered cubic cells was used. The number of k points was decreased proportionally as the number of cells increased in the supercell. The method of Methfessel-Paxton of order 1 was employed with a smearing value of 0.2. When atomic positions were fully relaxed, residual forces were lower than 0.02 eV/Å.

The calculations presented here consider ferromagnetic ground states because the small unit cell size enables a clear interpretation of the band structure. To analyze the band structures we fit the bands using maximally localized Wannier function [14] methods. Wannier functions were obtained using the WANNIER90 code [34] provided by the VASP package to project the VASP bands onto localized orbitals. We chose an energy window encompassing the p-d band complex and projected the Bloch functions onto p-symmetry orbitals centered on the O sites and d-symmetry orbitals centered on the transition-metal sites then minimized the MLWF spread. The resulting Wannier bands were in excellent agreement with the VASP bands. From the Wannier fits we then obtained on-site energies for the transition-metal d and oxygen p levels, as well as d-p hopping amplitudes.

We determined the charge transfer by comparing the integral of the valence band charge density (from the VASP output file CHGCAR) over the volume of each cubic subcell of the heterostructure to the corresponding values obtained from the individual LMO and LNO cells in the cubic and rocksalt structures.

IV. RESULTS: ENERGY BANDS AND DENSITY OF STATES

The four panels of Fig. 2 show the majority-spin energy bands of cubic $LaMnO_3$, cubic $LaNiO_3$, the $LaMnO_3/LaNiO_3$ 1/1 (001) superlattice the 1/1 (001) superlattice, and the rocksalt (double perovskite) La_2MnNiO_6.

Cubic $LaMnO_3$ is found to be metallic (obtaining insulating behavior requires including both the Jahn-Teller distortion and octahedral rotations). The bands that cross the Fermi level are about 4 eV wide and are of primarily Mn e_g origin (hybridized with $O_{p\sigma}$ orbitals lying about 2 eV below the Fermi level). These bands contain one electron shared between the two orbitals. In $LaNiO_3$ a similar situation occurs, but the rare-earth perovskite nickelates are negative-charge-transfer materials in which the $O_{2p\sigma}$ orbitals lie, in fact, at a slightly higher energy than the Ni e_g orbitals, implying, as will be seen in more detail below, that the bands crossing the Fermi level are p-d e_g-symmetry hybrids with majority-p character. The calculated band structure for the superlattice reveals a metallic state with two relatively wide bands that cross the Fermi level. As will be seen in more detail below, one of these bands arises from the Mn $d_{x^2-y^2}$ e_g state, and the other arises from the Ni p-d hybrid state of the same symmetry. Also visible just above the Fermi level is an unoccupied band mainly derived from the Mn-Ni antibonding combination of $d_{3z^2-r^2}$ e_g symmetry states (the bonding combination lies several eV below the Fermi level and is obscured by the many other orbitals in this energy range).

The metallic behavior of the superlattice may be understood as arising because the in-plane bands are only weakly affected by the superlattice formation. The wide energy range over which the bands disperse inhibits complete charge transfer. In fact, the net charge transferred from the Mn plane to the Ni plane is 0.4 e/unit cell. The calculated bands for the rocksalt structure reveal an insulator, essentially because in this structure both e_g orbitals on the Mn site mix strongly with the e_g orbitals on the Ni site, allowing splitting of all

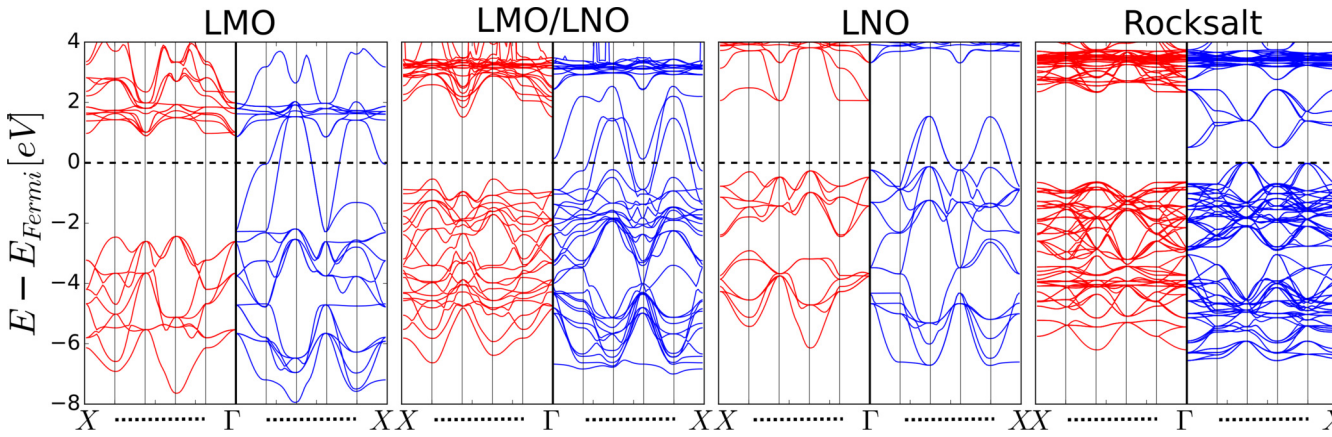

FIG. 2. Minority- (left subpanels) and majority-spin (right subpanels) bands of cubic $LaMnO_3$, $LaNiO_3$, the (001) $(LaNiO_3)_1/(LaMnO_3)_1$ superlattice, and the rocksalt (111) La_2MnNiO_6 double perovskite. All calculations are performed for ferromagnetic ground states using the GGA+U method as described in the text. The bands are plotted along the high-symmetry lines $\Gamma \rightarrow X \rightarrow R \rightarrow \Gamma \rightarrow M \rightarrow X$ of the Brillouin zone.

bands. The narrower bandwidth also promotes a larger charge transfer, approximately 0.7 e/unit cell.

To elucidate the physics revealed by our calculated band structures we consider the electronic density of states, projected onto given symmetry states of individual atoms. Figure 3 shows the orbitally projected densities of states for the cubic parent materials. From the top two panels we see that in $LaMnO_3$ the near-Fermi-surface states are e_g-symmetry antibonding d-p hybrids, with majority-d character. The corresponding bonding states are visible as the peak centered at ~ -7 eV. Comparison of the relative amplitude of bonding and antibonding states in the d and p partial density of states (DOS) confirms that the e_g d states lie above the p states in this material. The t_{2g}-symmetry states are fully filled and couple less strongly to the oxygen orbitals, as revealed by their smaller peak width and smaller bonding-antibonding splitting.

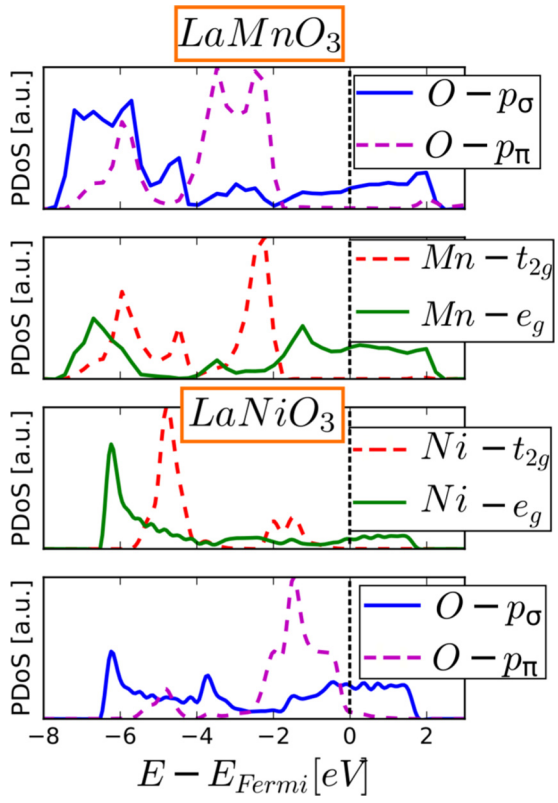

FIG. 3. Projection of the majority-spin density of states of ferromagnetic cubic $LaMnO_3$ and $LaNiO_3$ onto the transition-metal (Mn or Ni) d orbitals and onto oxygen p orbitals. The e_g-symmetry and t_{2g}-symmetry orbitals are plotted separately, as are the oxygen p_σ (hybridizing with the transition-metal e_g orbitals) and p_π (not hybridizing with the transition-metal e_g orbitals).

Turning now to the bottom two panels we see that for $LaNiO_3$ the Ni p-d manifold is somewhat narrower in energy than the p-d manifold in the Mn compound, reflecting a weaker p-d hybridization in the Ni material. We also see that most of the e_g-symmetry d density of states lies far below the Fermi level indicates that in $LaNiO_3$ the material is in the negative-charge-transfer class of materials in which the d states lie lower than the oxygen states and are further pushed down by p-d hybridization, as expected from the greater electronegativity of Ni relative to Mn and amply documented in the literature. As in the Mn compound the Ni t_{2g} states are fully filled and rather less strongly hybridized to the oxygen than the e_g states.

We now turn to the density of states of the superlattice, shown in Fig. 4. The top panel shows the density of states projected onto the oxygen states lying in the Mn-O plane, and the second panel shows the DOS projected onto the Mn states. Comparison to the corresponding panels of Fig. 3 shows that the superlattice-induced changes to the Mn-plane O orbitals and the Mn $d_{x^2-y^2}$ orbital are negligible. A splitting of the Mn $d_{3z^2-r^2}$ orbital is evident (leading, e.g., to the suppressed DOS at the Fermi level) with corresponding shifts to the "apical" (in-between Mn and Ni planes) oxygen orbital. Similarly, examination of the projection of the density of states onto the Ni and Ni-plane O orbitals reveals negligible changes to the planar orbitals; the small weight of the Ni d orbitals near the Fermi level makes changes in the Ni $d_{3z^2-r^2}$ orbitals difficult to discern. These results confirm that one of the bands that crosses the Fermi level is primarily of Mn $d_{x^2-y^2}$ character and the other is primarily of O character but within the Ni-O

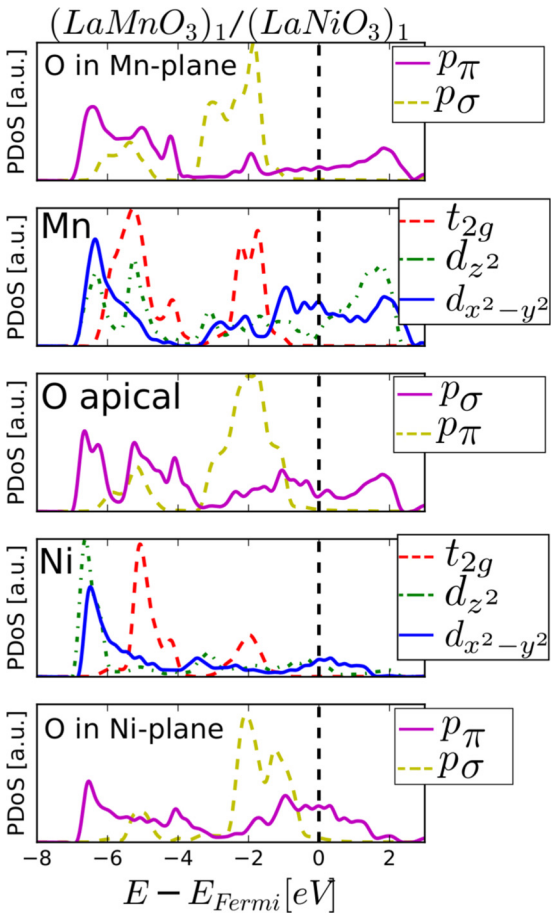

FIG. 4. Projection of the majority-spin density of states of the ferromagnetic $(LaNiO_3)_1/(LaMnO_3)_1$ superlattice onto the transition-metal (Mn or Ni) d orbitals and onto oxygen p orbitals. The two e_g orbitals are plotted separately, but all three t_{2g} orbitals are added together. The oxygen p_σ (hybridizing with the transition-metal e_g orbitals) and p_π (not hybridizing with the transition-metal e_g orbitals) are distinguished.

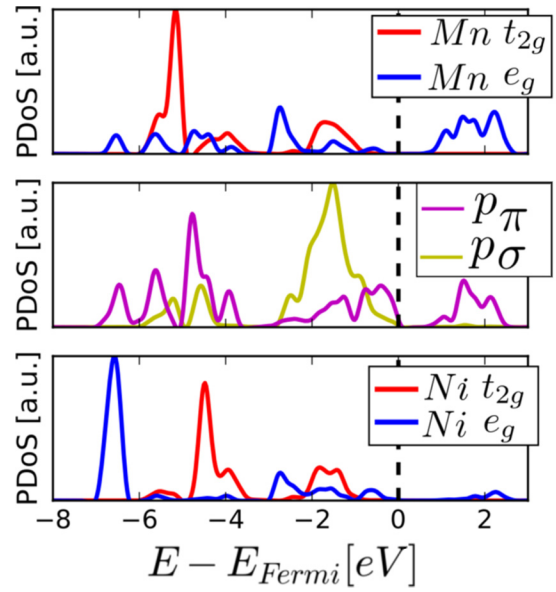

FIG. 5. Projections of the majority-spin density of states of ferromagnetic rocksalt $A_2BB'O_6$ onto e_g and t_{2g} orbitals are plotted separately. The oxygen p_σ (hybridizing with the transition-metal e_g orbitals) and p_π (not hybridizing with the transition-metal e_g orbitals) are distinguished.

plane, with the antibonding portion of the Mn $d_{3z^2-r^2}$ orbital and the O_{p_z} orbital split, with one portion pushed up in energy above the Fermi level by backscattering associated with the breaking of translational symmetry in the superlattice.

Finally, in Fig. 5 we show the partial densities of states for the rocksalt structure. The Mn d orbitals are now to a large degree pushed up above the Fermi level, and the Ni d orbitals and oxygen orbitals are submerged below, leading to insulating behavior and a larger degree of charge transfer.

V. PARAMETER TRANSFERABILITY: WANNIER ANALYSIS

Figure 2 shows that as the unit cell becomes larger, the number of energy bands increases, as does the band overlap, so the physics becomes more difficult to analyze. The bands would become even more complicated if octahedral rotations or antiferromagnetism were considered. For this reason, an important issue in analyzing the physics of nontrivial situations is parameter transferability, specifically, whether one can use parameters obtained in simpler situations to model more complicated ones. We have examined the transferability issue in the systems we consider by performing a MLWF analysis of our calculated bands for each of the structures. The MLWF analysis can be thought of as an unbiased determination of tight-binding parameters; a comparison of the parameters obtained for different situations then provides an estimate of transferability.

We find that the hopping amplitudes (interorbital matrix elements of the DFT+U Hamiltonian) between Mn or Ni and the coplanar O are the same within a few percent for all structures (e.g., the Mn e_g-O $2p_\sigma$ hopping is 1.7, and the Ni e_g-O $2p_\sigma$ hopping is 1.3 eV). We conclude that the hopping parameters are transferable.

The on-site energies (orbital-diagonal matrix elements of the DFT+U Hamiltonian) exhibit variation among systems. One contribution to the variation is changes to the combination of Madelung energies associated with different chemical environments as well as any electric fields arising from charge transfer (this is essentially the intrinsic contribution to the work function difference that gives rise to band bending at interfaces). For example, the photoemission data reported by Yoshimatsu *et al.* for $SrVO_3/SrTiO_3$ quantum wells [11,12] indicate an ∼0.9 eV shift in the oxygen energy from the one material to the other. A second contribution to the variation is a change in physics, in particular a variation of the p-d energy level splitting, which plays a crucial role in the physics of transition-metal oxides [35,36].

Table I presents the energies of the majority-spin Mn and Ni e_g-symmetry orbitals as well as the energies of the p_σ orbitals on different oxygen sites, distinguishing (for the layered structure) between oxygen states in the Mn or Ni plane and the apical oxygen sites that bridge the Mn and Ni planes. Table II presents the same information for the minority spin

TABLE I. Orbital energies obtained from maximally localized Wannier analysis for majority-spin band structures computed with $U_{Mn} = 4$, $U_{Ni} = 6$ eV, and $J = 1$ eV and measured relative to the Fermi level. Here $LaMnO_3$ and $LaNiO_3$ refer to the bulk compounds, SL refers to the 1/1 (001) superlattice and RS to the rock salt double perovskite structure.

Orbital	$LaMnO_3$	*SL*	RS	$LaNiO_3$
Mn_{z^2}	−2.2	−1.7	−1.1	
$Mn_{x^2-y^2}$	−2.2	−2.0	−1.4	
O:Mn plane	−4.6	−3.8	−2.3	
O:apical	−4.6	−3.4	−3.0	−2.8
Ni_{z^2}		−4.2	−4.0	1.6
$Ni_{x^2-y^2}$		−3.9	−4.0	1.6
O:Ni plane		−3.0	−2.3	−2.8

states. The "band-bending" or work function differences are clearly visible as differences between the energy of the O in the MnO_2 and NiO_2 planes. In addition, a change in the relative energies of the oxygen p and transition-metal d levels is apparent.

For cubic $LaMnO_3$ we have $E^{Mn}_{e_g} - E^{O}_{2p\sigma} \approx 2.4$ eV, while for $LaNiO_3$ we find $E^{Ni}_{e_g} - E^{O}_{2p\sigma} \approx -0.9$ eV, reflecting the negative-charge-transfer nature of the Ni compound. In the rocksalt structure we find $E^{Mn}_{e_g} - E^{O}_{2p\sigma} \approx 1.6$ eV, about 0.6 eV *less* than in bulk $LaMnO_3$, while $E^{Ni}_{e_g} - E^{O}_{2p\sigma} \approx -1.0$ eV, essentially unchanged from bulk $LaNiO_3$. In the superlattice we see that the energy difference between the average of the energies of the two Mn orbitals and the energy of the in-plane oxygen σ orbital $E^{Mn}_{e_g} - E^{O}_{2p\sigma} \approx 2.0$ eV. We thus conclude that the charge transfer energy is *not* transferable. The fact that the change is larger in the rocksalt than in the superlattice structure suggests that the d valence makes an important contribution to the p-d level splitting.

Interestingly, the p-d splitting on the Ni site is almost material independent. We attribute this to the negative-charge-transfer nature of the material, which implies (as can be seen from the density of states plot) that the near-Fermi-surface states are of primarily oxygen character. Thus in the approximation used here the actual charge density on the Ni sites changes only slightly (loosely speaking, the Ni-O plane goes from $d^8\bar{L}$ to d^8 as charges are added), and the mean valence of each of the three oxygens changes by less than $e/3$, so the oxygen Hartree shift is minimal, explaining why $\varepsilon_d - \varepsilon_p$ changes only slightly.

TABLE II. Orbital energies obtained from Maximally Localized Wannier analysis for minority spin band structures computed with $U_{Mn} = 4$, $U_{Ni} = 6$ eV. $J = 1eV$ and measured relative to the Fermi level. Here $LaMnO_3$ and $LaNiO_3$ refer to the bulk compounds, SL refers to the 1/1 (001) superlattice and RS to the rock salt double perovskite structure.

Orbital	$LaMnO_3$	*SL*	RS	$LaNiO_3$
Mn_{z^2}	−0.8	2.3	1.2	
$Mn_{x^2-y^2}$	−0.8	2.6	1.2	
O:Mn plane	−3.6	−4.1	−2.2	
O:apical	−3.6	−4.5	−3.2	−2.8
Ni_{z^2}		1.3	3.4	1.6
$Ni_{x^2-y^2}$		1.6	4.4	1.6
O:Ni plane		−3.0	−3.1	−2.8

Zhong and Hansmann [15] studied the dependence of the key $\varepsilon_d - \varepsilon_p$ parameter on charge transfer, focusing on compounds involving early and middle transition-metal oxides. Their observation that the ionization/affinity energies of transition-metal ions depend on the occupancy and thus affect band offsets and charge transfer is important. However, our results indicate that the statements in Ref. [15] that the p-d splitting scales with the product of the on-site U and charge transfer are not always correct. We find clear differences between the shifts on the Mn layer and the Ni layer, presumably related to the negative-charge-transfer nature of perovskite nickel oxide. Further, we find, in agreement with previous studies [36], that the double-counting correction to a large degree eliminates the Hartree shift, so within the formalism used here the connection between charge transfer, p-d splitting, and U cannot be as simple as that proposed by Zhong and Hansmann. Perhaps for this reason Eq. (3) of Ref. [15] relating the shift of p-level energies to charge transfer is not consistent with the data in Table I for either the Mn site or the Ni site. As a more minor point, we note that different d-level states and different oxygen ions behave differently: restricting our attention to "the [presumably orbitally averaged] d-level energy" and "oxygen energy" may gloss over important physics.

VI. COMPARISON TO EXPERIMENT

The essential features of the experiment of Hoffman *et al.* [13] are that for $(LaMnO_3)_n/(LaNiO_3)_n$ superlattices with $n \leqslant 2$ the ground state was insulating and an almost complete charge transfer of one electron occurred from Mn to Ni. These behaviors are not reproduced by the calculations, which predict that even for the $n = 1$ superlattice we have metallic behavior with $\sim 0.4e$ charge transfer. The two effects are closely related: the planar orbitals ($d_{x^2-y^2}$ and in-plane p_σ) are only minimally affected by superlattice formation, and the resulting bandwidths are so large that the moderate Mn-Ni electronegativity difference cannot empty the Mn d bands. While our calculations are based on the DFT+U approximation, a Hartree approximation to a complicated many-body situation, we believe that correcting the deficiencies of this approximation is unlikely to change the basic theoretical prediction because the conclusion arises from eV-scale energetics of different valence states, which are well captured by DFT/Hartree approximations.

The results presented here were derived from idealized cubic-type structures; however, we have also investigated the consequences of changing the structure. Changing the lattice parameter of the cells to those of LNO or LMO changes only the dispersion of the electronic states. Modifying the spin orientation on the Mn and Ni sites to the antiferromagnetic coupling does not open a full band gap in any of the heterostructures considered: the $d_{x^2-y^2}$ band remains metallic in all cases. For the model (1,1) superlattice presented in the previous section, all internal coordinates were fully relaxed with VASP, keeping the unit cell parameters fixed. The initial

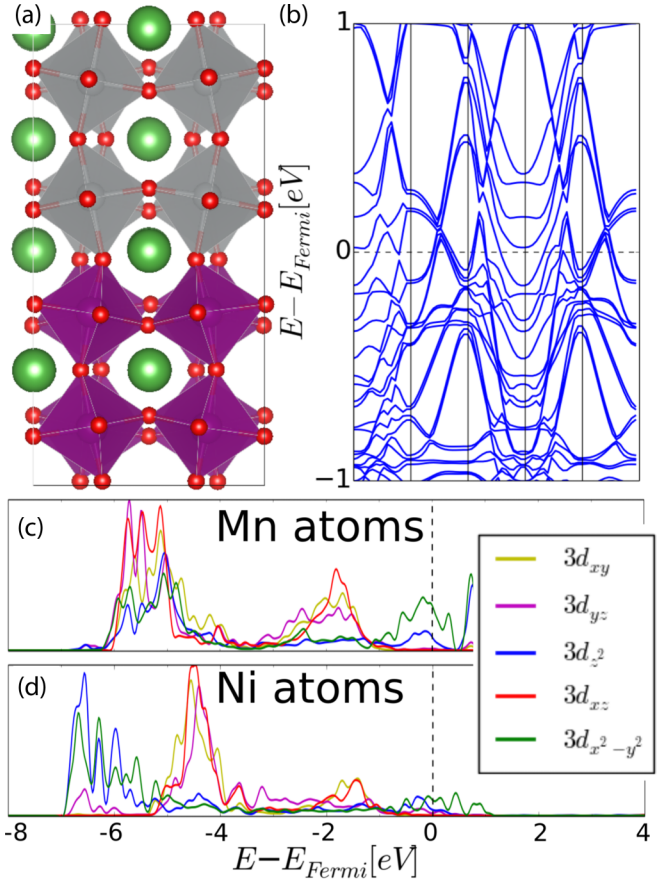

FIG. 6. (a) Schematic representation of the relaxed cubic $(LaNiO_3)_2/(LaMnO_3)_2$ heterostructure. (b) Band structure of the majority spin. The projected DOS onto the d orbitals of the two types of nonequivalent Mn atoms is plotted in (c) and (d). The bands are plotted along the high-symmetry lines $\Gamma \rightarrow X \rightarrow R \rightarrow \Gamma \rightarrow M \rightarrow X$ of the Brillouin zone.

condition was taken to be the ideal tetragonal structure cell. In the relaxed structures all forces were less than 1 meV/Å. The physics of the relaxed structures was not materially different from the physics of the unrelaxed structures with moderate charge transfer and wide metallic bands derived from the e_g orbitals crossing the Fermi level.

Another possibility is that the electron transfer and differing hybridization strengths will cause motion of the apical oxygen away from Ni and towards Mn. However, relaxing the internal coordinates leads to only an ∼0.1 Å shift in the apical O position, too small to change the energetics significantly. We also investigated variant structures in which the apical O is displaced by 0.2 and 0.4 Å toward Mn. The charge transfer increases to 0.53 and 0.7 electron, respectively, but the $d_{x^2-y^2}$-derived orbitals remain partially occupied, and the superlattice remains metallic.

Interestingly, the rocksalt structure has a similar $0.7e$ charge transfer but is insulating, essentially because the backscattering associated with the Mn-Ni alternation opens a band gap. We conclude that the insulating behavior requires disruption of the in-plane Mn-O and Ni-O networks and speculate that a high density of Mn/Ni antisite defects in the near-interface layers could disrupt the in-plane networks as well as promoting larger charge transfer, thus producing physics similar to that found in the calculations of the rocksalt structure. In this regard it is interesting to note that evidence of substantial Ni-Mn intermixing, especially for the near-substrate layers, was very recently reported in a closely related superlattice [37].

Finally, we consider the $(LaNiO_3)_2/(LaMnO_3)_2$ superlattice with a $2 \times 2 \times 4$ computational unit cell, which allows for two-sublattice charge and Jahn-Teller order on the Mn and Ni layers. The band structure is shown in Fig. 8. All internal degrees of freedom were fully relaxed with VASP until forces were less than 1 meV/Å. We started from two initial conditions: the pseudocubic structure considered above and a structure in which LMO has the bulk LMO two-sublattice Jahn-Teller order and the LNO has no order. For both sets of initial conditions and all U values, we find that there are also modest octahedral rotations and a weak two-sublattice Jahn-Teller-like structural distortion, but the hybrid structure remains metallic, with numerous bands crossing the Fermi level. A projected DOS analysis [see Figs. 6(c) and 6(d)] demonstrates that in this structure the metallic behavior arises primarily from the wide $d_{x^2-y^2}$ bands of both the Mn and Ni sublattices.

Other attempts to reproduce the experimental band gap starting with different geometries and $+U$ values were also conducted. Two different sets of $+U$ parameters were considered: $U_{Mn} = 2$, $U_{Ni} = 4$ and $U_{Mn} = 8$, $U_{Ni} = 6$. In both cases, a $2 \times 2 \times 2$ cubic supercell of LNO was placed on the top of an already relaxed $2 \times 2 \times 2$ supercell of LMO with appropriate Jahn-Teller distortions, yielding a metallic band diagram. Geometries were allowed to fully relax, leading to final structures rather similar to the one in Fig. 6 for both sets of $+U$ parameters. In both cases the LNO sublattice followed the distortion of the LMO, which in turn did not change to a cubic geometry, as reported in experiments. Energy band diagrams are displayed in Fig. 8 in the Appendix.

VII. CONCLUSIONS

First-principles calculations of model $LaMnO_3$ and $LaNiO_3$ structures reveal that the basic physics of the superlattice situation is controlled by geometry, which determines hopping amplitudes and thus band structures, and by relative electronegativity of the transition-metal ions, which determines charge transfer. Our calculations strongly suggest that in the ideal superlattice, the wide $d_{x^2-y^2}$-symmetry bands are essentially unaffected by superlattice formation and remain metallic because the Mn-Ni electronegativity difference is smaller than the bandwidth, so the Mn-derived bands remain partly occupied and the Ni-derived bands remain partly empty. This should be contrasted with $LaTiO_3/LaNiO_3$ superlattices studied previously. Theoretical calculations predict [38] and experiment confirms [39] that in $LaNiO_3/LaTiO_3$ superlattices, one electron is transferred from the $LaTiO_3$ layer to the $LaNiO_3$ layer, hanging the formal valence to a configuration similar to that of rocksalt NiO, a well-known Mott/charge transfer insulator, and producing insulating behavior. In this system this happens because the Ti-Ni electronegativity difference is large enough and the Ti d_{xy} band is narrow enough that nearly complete charge transfer occurs. We also note the $SrVO_3/SrTiO_3$ superlattices modeled by Zhong *et al.* [10] in

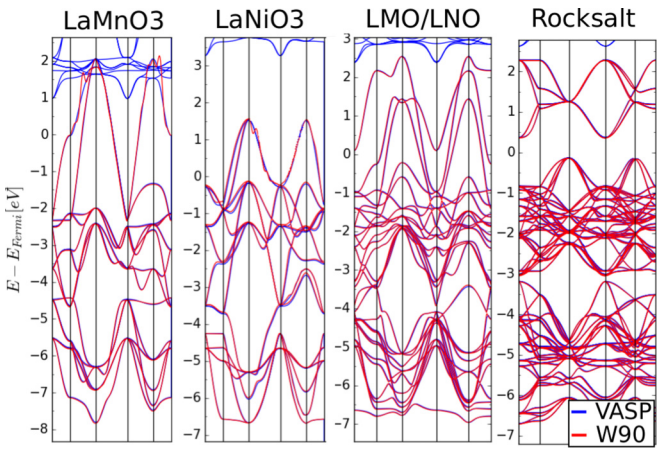

FIG. 7. Comparison of the first-principles-obtained band structure with the WANNIER90-interpolated band structure for cubic $LaMnO_3$, cubic $LaNiO_3$, the $(LaNiO_3)_1/(LaMnO_3)_1$ heterostructure, and ferromagnetic rocksalt.

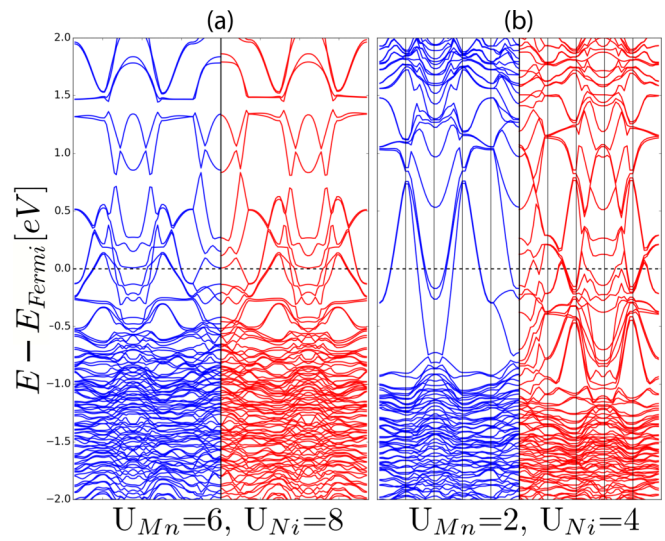

FIG. 8. Minority- (left subpanels) and majority-spin (right subpanels) bands of the $2 \times 2 \times 4\,(LaNiO_3)_2/(LaMnO_3)_2$ heterostructure for different sets of $+U$ values ($J = 1$). (a) $U_{Mn} = 6$, $U_{Ni} = 8$ and (b) $U_{Mn} = 2$, $U_{Ni} = 4$. The bands are plotted along the high-symmetry lines $\Gamma \to X \to R \to \Gamma \to M \to X$ of the Brillouin zone.

which there is essentially no charge transfer and the physics is of dimensionality reduction and confining potentials.

An analysis based on maximally localized Wannier functions demonstrates that transition-metal/oxygen hybridization amplitudes and oxygen site energies are transferable, so that parameters derived from calculations performed in simple geometries can be used in phenomenological models of more complex situations. However, the transition-metal d-oxygen p level splitting is not transferable: it is found to depend on the charge transfer, essentially because the transition-metal electronegativity depends on d occupancy.

For the LMO/LNO system that motivated our study, we found that within our theoretical framework the only viable explanation for the observed insulating behavior of thin superlattices was a large concentration of antisite defects, essentially because of the partial charge transfer leading to partial filling of the relatively wide planar (x^2-y^2-derived) bands. Note that our structural relaxations indicate that octahedral rotations are far from being large enough to narrow the bands and eliminate band overlap. Some experimental evidence for antisite defects has recently been reported [37]. As a possible alternative, we note that it is conceivable that some other mechanism (e.g., thermal fluctuations at higher temperatures) might lead to octahedral rotations with a much larger amplitude than considered here, perhaps reducing the bandwidth in the layered structures enough to eliminate the overlap between bands, thereby allowing a larger charge transfer, leading to insulating behavior. Experimental investigation of antisite defects and of octahedral rotations would be valuable.

We suggest directions for future theoretical research. First, the charge transfer depends on the difference in electronegativity, as also noted by Zhong and Hansmann [15] (although as explained above, the details of our findings are not in complete agreement with theirs). The DFT+U approach used here provides an approximation to the electronegativity difference. The issue also relates to basic questions of the double counting in the $+U$ methodology. Further studies of these issues by other methods would be valuable. Second, here parameter transferability has been investigated in one particular material system. We conjecture that the main result (transfer of all parameters except for the p-d level splitting) will extend to all transition-metal oxides heterostructures, but further investigation would be desirable. Perhaps most importantly, it appears from our results that the difference between the energies of the p and d orbitals of the Mn cation is not transferable between structures and that change in the p-d splitting in late transition-metal oxides (e.g., the Ni compound we studied) may be different than in the early transition-metal ions.

ACKNOWLEDGMENTS

This work was supported by the US Department of Energy, Office of Science, Basic Energy Sciences, Materials Science and Engineering Division. We acknowledge the computing resources provided on Bebop, the high-performance computing clusters operated by the Laboratory Computing Resource Center at Argonne National Laboratory.

APPENDIX: WANNIER ANALYSIS

To obtain model Hamiltonians we resort to the maximally localized Wannier functions (MLWFs) [14], obtained using the WANNIER90 code [34] from the first-principles ground state obtained with VASP. By projecting onto p and d orbitals and minimizing the MLWF spread, the band structure obtained using the first-principles approach compared to the Wannier interpolation were in excellent agreement. Figure 7 shows a comparison of the four structures of interest.

[1] J. Chakhalian, J. W. Freeland, A. J. Millis, C. Panagopolous, and J. M. Rondinelli, Rev. Mod. Phys. **86**, 1189 (2014).

[2] M. Imada, A. Fujimori, and Y. Tokura, Rev. Mod. Phys. **70**, 1039 (1998).

[3] Y. Tokura, Rep. Prog. Phys. **69**, 797 (2006).

[4] T. Kimura and Y. Tokura, Annu. Rev. Mater. Sci. **30**, 451 (2000).

[5] S. Middey, J. Chakhalian, P. Mahadevan, J. Freeland, A. Millis, and D. Sarma, Annu. Rev. Mater. Res. **46**, 305 (2016).

[6] M. Gibert, P. Zubko, R. Scherwitzl, J. Iniguez, and J.-M. Triscone, Nat. Mater. **11**, 195 (2012).

[7] C. Piamonteze, M. Gibert, J. Heidler, J. Dreiser, S. Rusponi, H. Brune, J.-M. Triscone, F. Nolting, and U. Staub, Phys. Rev. B **92**, 014426 (2015).

[8] J. D. Hoffman, B. J. Kirby, J. Kwon, G. Fabbris, D. Meyers, J. W. Freeland, I. Martin, O. G. Heinonen, P. Steadman, H. Zhou, C. M. Schlepütz, M. P. M. Dean, S. G. E. te Velthuis, J.-M. Zuo, and A. Bhattacharya, Phys. Rev. X **6**, 041038 (2016).

[9] A. T. Lee and M. J. Han, Phys. Rev. B **88**, 035126 (2013).

[10] Z. Zhong, Q. Zhang, and K. Held, Phys. Rev. B **88**, 125401 (2013).

[11] K. Yoshimatsu, T. Okabe, H. Kumigashira, S. Okamoto, S. Aizaki, A. Fujimori, and M. Oshima, Phys. Rev. Lett. **104**, 147601 (2010).

[12] K. Yoshimatsu, K. Horiba, H. Kumigashira, T. Yoshida, A. Fujimori, and M. Oshima, Science **333**, 319 (2011).

[13] J. Hoffman, I. C. Tung, B. B. Nelson-Cheeseman, M. Liu, J. W. Freeland, and A. Bhattacharya, Phys. Rev. B **88**, 144411 (2013).

[14] N. Marzari and D. Vanderbilt, Phys. Rev. B **56**, 12847 (1997).

[15] Z. Zhong and P. Hansmann, Phys. Rev. X **7**, 011023 (2017).

[16] H. Chen and A. Millis, Phys. Rev. B **93**, 104111 (2016).

[17] T. Mizokawa, D. I. Khomskii, and G. A. Sawatzky, Phys. Rev. B **61**, 11263 (2000).

[18] M. J. Han, X. Wang, C. A. Marianetti, and A. J. Millis, Phys. Rev. Lett. **107**, 206804 (2011).

[19] H. Park, A. J. Millis, and C. A. Marianetti, Phys. Rev. Lett. **109**, 156402 (2012).

[20] S. Johnston, A. Mukherjee, I. Elfimov, M. Berciu, and G. A. Sawatzky, Phys. Rev. Lett. **112**, 106404 (2014).

[21] P. W. Anderson and H. Hasegawa, Phys. Rev. **100**, 675 (1955).

[22] A. J. Millis, P. B. Littlewood, and B. I. Shraiman, Phys. Rev. Lett. **74**, 5144 (1995).

[23] J. Kanamori, J. Appl. Phys. **31**, S14 (1960).

[24] J. B. A. A. Ellemans, B. van Laar, K. R. van der Veen, and B. O. Loopstra, J. Solid State Chem. **3**, 238 (1971).

[25] A. M. Zhang, S. L. Cheng, J. G. Lin, and X. S. Wu, J. Appl. Phys. **117**, 17B325 (2015).

[26] C. Franchini, R. Kováčik, M. Marsman, S. S. Murthy, J. He, C. Ederer, and G. Kresse, J. Phys.: Condens. Matter **24**, 235602 (2012).

[27] E. A. Nowadnick, J. P. Ruf, H. Park, P. D. C. King, D. G. Schlom, K. M. Shen, and A. J. Millis, Phys. Rev. B **92**, 245109 (2015).

[28] P. E. Blöchl, Phys. Rev. B **50**, 17953 (1994).

[29] J. P. Perdew, K. Burke, and M. Ernzerhof, Phys. Rev. Lett. **77**, 3865 (1996).

[30] S. L. Dudarev, G. A. Botton, S. Y. Savrasov, C. J. Humphreys, and A. P. Sutton, Phys. Rev. B **57**, 1505 (1998).

[31] G. Kresse and J. Hafner, Phys. Rev. B **48**, 13115 (1993).

[32] G. Kresse and J. Furthmüller, Phys. Rev. B **54**, 11169 (1996).

[33] G. Kresse and D. Joubert, Phys. Rev. B **59**, 1758 (1999).

[34] A. A. Mostofi, J. R. Yates, Y.-S. Lee, I. Souza, D. Vanderbilt, and N. Marzari, Comput. Phys. Commun. **178**, 685 (2008).

[35] J. Zaanen, G. A. Sawatzky, and J. W. Allen, Phys. Rev. Lett. **55**, 418 (1985).

[36] H. T. Dang, A. J. Millis, and C. A. Marianetti, Phys. Rev. B **89**, 161113 (2014).

[37] J.-H. Kwon, J. Horrman, R. Yuan, A. Yoon, A. Bhattacharya, and J.-M. Zuo, Semicond. Sci. Technol. **32**, 014002 (2017).

[38] H. Chen, A. J. Millis, and C. A. Marianetti, Phys. Rev. Lett. **111**, 116403 (2013).

[39] Y. Cao, Z. Yang, M. Kareev, X. Liu, D. Meyers, S. Middey, D. Choudhury, P. Shafer, J. Guo, J. W. Freeland, E. Arenholz, L. Gu, and J. Chakhalian, Phys. Rev. Lett. **116**, 076802 (2016).